Geomechanics and Engineering, *Vol. 27, No. 2 (2021) 131-150*
https://doi.org/10.12989/gae.2021.27.2.131

Impact of grain size or anisotropy on correlations between rock tensile strength and some rock index properties

Fanmeng Kong, Yiguo Xue*, Daohong Qiu, Zhiqiang Li, Qiqi Chen and Qian Song

Geotechnical and Structural Engineering Research Center, Shandong University, No. 17923 of Jingshi Road, Jinan City, China

(Received April 23, 2020, Revised April 29, 2021, Accepted October 6, 2021)

Abstract. Brazilian tensile strength (BTS) is a critical mechanical parameter of rock; and the measurement of BTS performed on core samples is a cumbersome procedure. Thus, rock index properties including point load, P-wave velocity and Schmidt hammer tests have been widely used to estimate BTS. The correlations between BTS and index properties are rock-type, grain size and anisotropy dependent, but, how the correlations related to the variation of grain size or anisotropy remain unexplained. In this study, the impact of grain size or anisotropy on those correlations is respectively examined using sandstone (fine or coarse grain size) and gneiss (0°, 45°, 90° inclined anisotropy) samples. Several significant equations for predicting BTS through index properties were established for different types of samples. The finding implies that either grain size variation or multidirectional anisotropy reduces not only the correlated degree between BTS and index properties, but also the BTS estimation reliability of those empirical equations. All three index properties should be used with much care for coarse-grained rock and respectively performed on samples with unidirectional anisotropy. Using an empirical equation between BTS and index properties ignoring grain size or anisotropy can yield considerable discrepancies of estimated BTS. Among three index properties, point load test is the first choice for predicting BTS as the small discrepancies of estimated results. As the invalid correlation, P-wave velocity test should not be performed at 45° angle to the anisotropy in the BTS estimation; and this recommendation is also appropriate for Schmidt hammer test conducted parallel to anisotropy.

Keywords: anisotropy; Brazilian tensile strength; correlations; grain size; rock index properties

1. Introduction

Rock exhibits inferior resistance to tensile stress and tensile cracks are more easily initiated, propagated and observed (Liu *et al*. 2014, Komurlu *et al*. 2016, Yao *et al*. 2018, Wei *et al*. 2020, Xue *et al*. 2021). Tensile strength, thus, is one of the extremely significant factors to characterize the failure property of rock or rock mass (Perras and Diederichs 2014, Shang *et al.* 2016, Wang and Hu 2017). Also, tensile stress zones are widespread throughout rock mass involved in underground-related activities such as tunnelling, mining, disposal of radioactive waste and underground oil storage (Cai and Kaiser 2005, Wang *et al.* 2007, Shen and Barton 2018). As such, tensile strength of rock is of particular interest to the perspective of rock mechanics.

The tensile strength can be measured using the direct tensile test, Brazilian test or three-point-bend test in the laboratory. Performing a direct tensile test requires high-quality rock specimen and may generate a significant error due to stress concentration derived from gripping of the rock specimens and misalignment (Xia *et al.* 2017). In 1978, the International Society for Rock Mechanics (ISRM 1978) officially proposed the Brazilian test to determine the tensile strength of rock materials. This method was later recommended by many countries (e.g. American Society for Testing Material (ASTM 2008) or China National Standard (2013)) for the standard measurement of tensile strength. Both the experimental procedure or environmental factors exert considerable effects on the rock tensile strength. For example, the results of Brazilian test depend not only on the contact condition between the specimen and steel loading jaws, but also on whether the crack initiates at the center of specimen (Erarslan and Williams 2012). Moreover, rock tensile strength can be significantly lowered by saturation, freeze-thaw cycles and heat treatment (Roy and Singh 2016, Sirdesai *et al.* 2016, Roy *et al.* 2017, Zhao *et al.* 2017, Liu *et al.* 2018, Kumari *et al*. 2019).

At present, Brazilian tensile strength (BTS) has been widely referenced in rock engineering projects. The direct measurement of Brazilian tensile strength (BTS) relies on certified experiment apparatus and high-quality core samples (Tutmez 2018). One challenge is that standard core sample preparation can be expensive and time-consuming, especially for the extremely soft, hard, highly fractured, laminated and coarse granular sedimentary rocks (Komurlu *et al.* 2017, Kong and Shang 2018, Aliyu *et al.* 2019, Kong *et al.*2021). As such, the index tests (referred to point load, P-wave velocity and Schmidt hammer test, etc.) have been widely used to estimate the BTS (Kahraman *et al.* 2018). This is because the simple testing apparatus and optional rock specimens, such as core, block or irregular lump specimens for point load test. More recently, to timely

*Corresponding author, Professor
E-mail: xieagle@sdu.edu.cn

http://www.techno-press.org/?journal=gae&subpage=7
ISSN: 2005-307X (Print), 2092-6219 (Online)

determine the proper tunnelling parameters of TBM (Tunnel Boring Machine), point load index through irregular rock lumps from TBM cutter has been recognized as the first-order choice for estimating rock strength.

Predicting BTS through index tests has received significant attention since 1990s. One of the pioneering studies on this topic was reported by Butenuth (1997), where four charts were developed for comparing the tensile strength with the point load index. The establishment of those charts was based on the published data of sandstones, marble and granite. Mishra and Basu (2012) also compared the BTS estimation performance of the point load test with block punch test. They found these two tests revealed similar importance for calculating BTS through linear equations. Moreover, several academics attempted to extend the study of using point load index ($I_{s(50)}$) to predict BTS for special rocks such as gypsum (referred to particular deformation behaviour) and meta-siltstone/sandstone (with extremely high strength) (Heidari *et al.* 2012, Li and Wong 2013). All of them reported linear equations for correlating BTS to $I_{s(50)}$; and those equations possessed acceptable reliability for the preliminary design of rock engineering projects.

For the ultrasonic pulse velocity test (P-wave velocity, V_P), Khandelwal and Singh (2009) were the pioneers who used this method to estimate BTS for coal measure rocks. They reported a linear relationship between BTS and V_P; and this relationship could be used to calculate BTS of coal measure rocks for the design of mining projects. After intensive laboratory experiments and regression analyses, Karakul and Ulusay (2013) proposed several power equations for inferring BTS from V_P. They found that the empirical correlations could yield under or over-prediction of BTS of rocks with different degrees of saturation. Thus, the polynomial equations with high prediction performance were developed using multivariate statistical analysis, whereby recognizing the parameters including V_P, effective clay content and degree of saturation. Apart from the frequently-used regression analysis, Singh *et al.* (2017) brought attention to extending Artificial Neural Network (ANN) for use to estimate BTS by V_P, which indicated that the effectiveness of ANN over simple regression analysis.

In addition, the Schmidt hammer test has also been used for estimating BTS of rock materials because of the quick, portable and non-destructive testing equipment. The relations between BTS and Schmidt hammer rebound number (R) have been presented through various methods such as simple regression analysis, multivariate statistical analysis or ANN model (Kılıç and Teymen 2008, Gurocak *et al.* 2012, Karaman *et al.* 2015).

Brazilian test and index properties have grain size or anisotropy (referred to bedding, schistosity, gneissosity, microfissure) dependent nature (Jamshidi *et al.* 2018, Shang 2020). For example, Khanlari *et al.* (2014b) point out that the maximum BTS can be obtained when the Brazilian test is performed normal to the anisotropy, but, the minimum BTS is obtained at different anisotropy inclinations in different rock samples. The point load test results may also vary significantly following the various anisotropy orientations and the most reliable strength index can be seen from the sample with horizontal anisotropy (Broch 1983). Moreover, Schmidt hammer readings are more discrete for rock containing coarse grains with sizes comparable to the diameter of hammer plunger tip (Aydin 2009).

However, the isotropic and homogeneous rocks are theoretical assumptions seldom found in nature. Using empirical equation between BTS and index properties for rock with different grain-size or anisotropic characteristics can generate considerable errors, e.g., overestimating BTS with a discrepancy of 295.7% (data from Karaman *et al.* 2015). Up to now, the impact of grain size or anisotropy on the results of Brazilian, point load, P-wave velocity and Schmidt hammer test has been widely discussed by researchers. Also, many different equations have been proposed to calculate BTS by index properties for different rocks (Table 1). However, how these correlations respond to the grain size or anisotropy orientation has not yet been explained and published.

To offer instructions for using index properties to estimate BTS of anisotropic or heterogeneous rock, the influence of grain size or anisotropy on the correlations between BTS and index properties was respectively investigated in this study. As such, the impact of grain size or anisotropy on the empirical correlations can be minimized and the accuracy of estimated BTS can be consequently upgraded.

Fine or coarse-grained sandstones (definitely same rock-type) and gneisses (with visible anisotropy) were sampled from different locations of China, followed by presenting standard Brazilian test as well as point load, P-wave velocity and Schmidt hammer test in the laboratory. Regression analysis was subsequently used to develop the equations for estimating BTS by index tests. After that, the impact of grain size or anisotropy on those proposed equations was respectively explored by interpreting the regression analysis parameters and BTS estimation capabilities of equations. A comparison study was finally performed by comparing the correlations of this study with previous results.

2. Materials and methods

2.1 Sample selection and specimen preparation

Sandstone and gneiss blocks were sampled in two regions in China (Fig. 1). They are Zibo sandstone and Jining gneiss. The homogeneous sandstones were sampled in identical Carboniferous stratigraphic section to enable the same rock-type, where the lithological effect could be eliminated. To clearly display the impact of grain size, sandstone blocks contained two groups: fine-grained size (< 0.1 mm) and coarse-grained size (> 0.25 mm) (site A in Fig. 1). Differences in grain size can be noted in the thin section photomicrographs of the sandstones (Figs. 2(a)-(d)). The gneisses were formed in the geological age of Neo-archean (site B in Fig. 1) and characterized by a clear gneissic structure referring to a representative anisotropy (Figs. 2(e)-(f)).

Table 1 Previous equations between BTS (MPa) and index tests

Formulations	Rock types	No. of samples (specimens) tested	References
BTS=7.5Ln($I_{s(50)}$) + 2.22 (R^2=0.93)	Southern Anatolia limestone, tuff, sandstone, diorite, quartzite (Turkey)	19 specimens	Kılıç and Teymen (2008)
BTS=1.569$I_{s(50)}$ + 1.514 (R^2=0.54)	Granite, andesite, basalt, sandstone, gypsum, marble (Turkey)	121 specimens	Yilmaz (2010)
BTS=4.78$I_{s(50)}$ + 1.81 (R^2=0.81)	Granite, basalt, limestone, siltstone, marble, etc. (Turkey)	686 samples	Gurocak et *al.* (2012)
BTS=1.3584$I_{s(50)}$ + 2.0607 (R^2=0.93)	Gachsaran Formation gypsum (Turkey)	15 specimens	Heidari et *al.* 2012
BTS=0.81$I_{s(50)}$ + 7.96 (R^2=0.59)	Granite (India)		
BTS=1.96$I_{s(50)}$ + 4.84 (R^2=0.69)	Schist (India)	20 specimens	Mishra and Basu (2012)
BTS=1.1$I_{s(50)}$ + 1.25 (R^2=0.82)	Sandstone (India)		
BTS=0.94$I_{s(50)}$	Jurong Formation meta-siltstone (Singapore)	12 samples (118 specimens)	Li and Wong (2013)
BTS=0.66$I_{s(50)}$	Jurong Formation meta-sandstone (Singapore)		
BTS=2.20$I_{s(50)}^{0.79}$	Hornfels, phyllite, slate, schist (Iran)	35 samples	Khanlari et *al.* (2014a)
BTS=3.34$I_{s(50)}$ − 3.4 (R^2=0.90)	Basalt, dacite, limestone, metabasalt, volcanic breccia (Turkey)	47 specimens	Karaman et *al.* (2015)
BTS=2.28$I_{s(50)}$ − 4.66 (R^2=0.95)	Hornfelsic rocks (Iran)	8 samples (320 specimens)	Fereidooni (2016)
BTS=0.8261$I_{s(50)}$ − 0.9243 (R^2=0.72)	Sandstone, limestone, travertine, conglomerate (Iran)	12 samples	Fereidooni and Khajevand (2018)
BTS=0.74$I_{s(50)}$ (R^2=0.91)	Yanshan orogeny biotitic monzogranite (China)	15 samples (84 specimens)	Xue et *al.* (2020)
BTS=0.493$V_p^{1.872}$(km/s) (R^2=0.92)	Southern Anatolia limestone, tuff, sandstone, diorite, quartzite, marble, granodiorite (Turkey)	19 specimens	Kılıç and Teymen (2008)
BTS=0.0145V_P − 24.55 (m/s) (R^2=0.95)	Sandstone, shale, coal (India)	12 samples	Khandelwal and Singh (2009)
BTS=1.050$V_p^{1.389}$ (km/s) (R^2=0.75)	Dry andesite, tuff, sandstone, marl (Turkey)	14 samples	Karakul and Ulusay (2013)
BTS=0.583$V_p^{1.473}$ (km/s) (R^2=0.71)	Saturated andesite, tuff, sandstone, marl (Turkey)		
BTS=0.001V_P + 0.662 (m/s) (R^2=0.88)	Granite, sandstone, limestone, dolomite, marble (India)	13 samples	Khandelwal (2013)
BTS=0.0054V_P − 8.3622 (m/s) (R^2=0.84)	Schist, basalt, limestone, gneiss, quartzite, dolomite, shale and sandstone (India)	-	Singh *et al.* (2017)
BTS=0.0087$R^{1.7757}$ (R^2=0.94)	Southern Anatolia limestone, tuff, sandstone, diorite, quartzite, marble, granodiorite (Turkey)	19 specimens	Kılıç and Teymen (2008)
BTS=9.07R − 375.55 (R^2=0.59)	Igneous, sedimentary, metamorphic rocks (Turkey)	686 samples	Gurocak *et al.* (2012)
BTS=0.72R − 16.6 (R^2=0.85)	Basalt, dacite, limestone, metabasalt, volcanic breccia (Turkey)	47 specimens	Karaman *et al.* (2015)
BTS=3.5×10$^{-6}R^{3.80}$ (R^2=0.92)	Hornfelsic rocks (Iran)	8 samples (320 specimens)	Fereidooni (2016)
BTS=0.2808R − 2.0232 (R^2=0.67)	Sandstone, limestone, travertine, conglomerate (Iran)	12 samples	Fereidooni and Khajevand (2018)

Note: $I_{s(50)}$ (MPa) is the point load index; V_P is the P-wave velocity; R is the Schmidt hammer rebound number; R^2 is the correlation coefficient

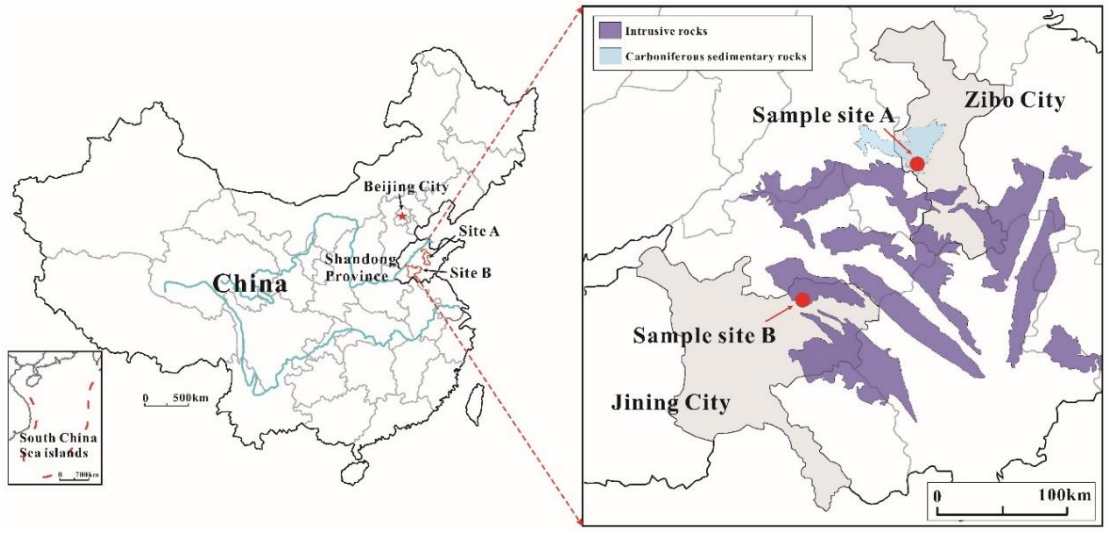

Fig. 1 The locations of rocks used in this study. Data from the China Geological Survey (2019)

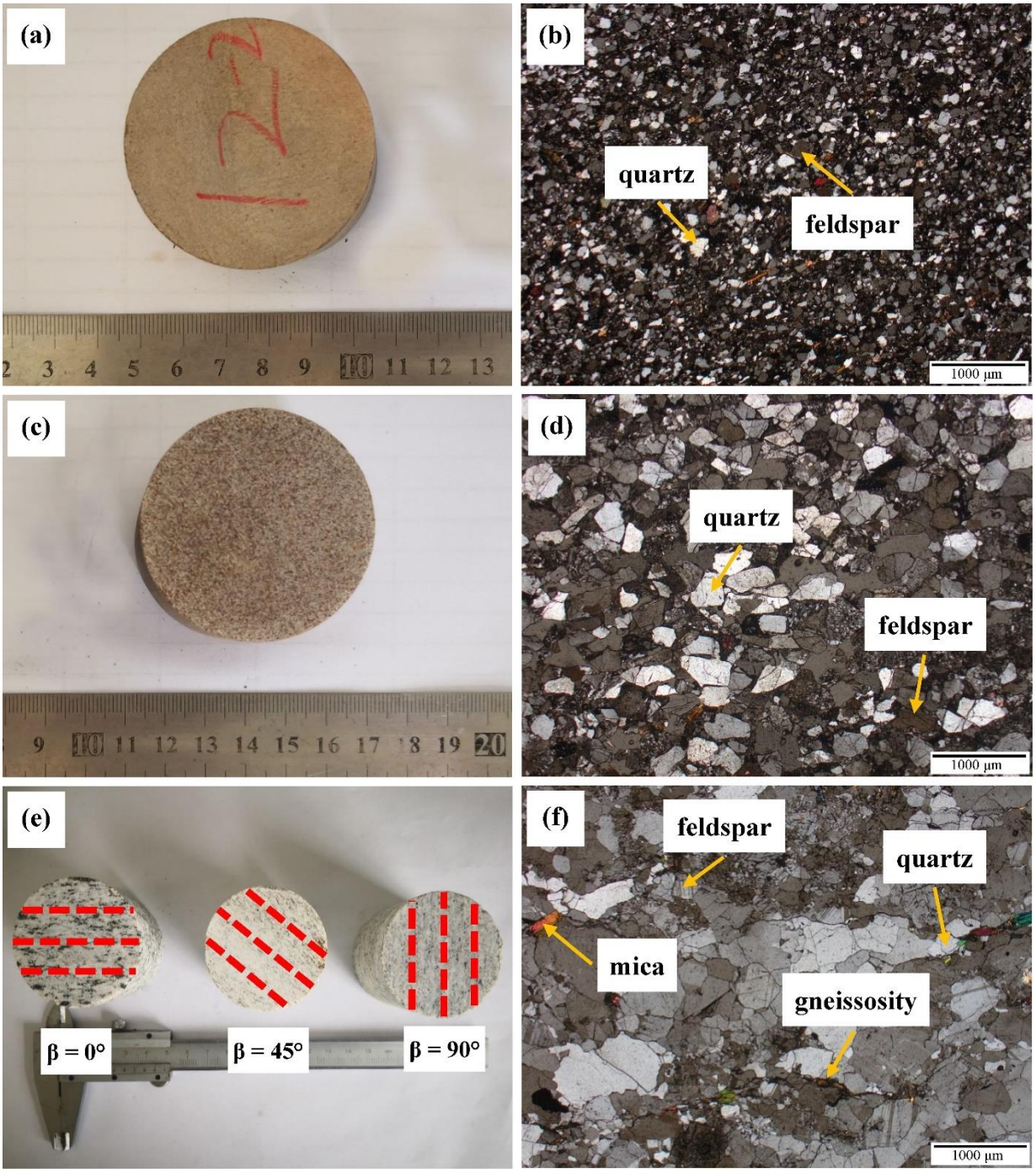

Fig. 2 The characterization of rock samples used in this study. (a) fine-grained sandstone samples; (b) section photomicrographs of fine-grained sandstone under cross-polarized light; (c) coarse-grained sandstone samples; (d) section photomicrographs of coarse -grained sandstone under cross-polarized light; (e) gneiss samples; (f) section photomicrographs of gneiss under cross-polarized light

In the preparation of the cylindrical specimens, the drilling sampler with a diameter of 50 mm was used. Ends of the cylindrical specimens were ground flat using emery. To consider the impact of anisotropy inclination-β (i.e., the angle between anisotropy planes and horizontal direction in degree) on empirical equations for estimating BTS, gneiss cores were drilled normal, at 45° angle or parallel to the anisotropy (i.e., β = 0°, 45° or 90°). Some representative rock samples are shown in Fig. 2(a), (c) and (e).

2.2 Experimental scheme

All the laboratory experiments were conducted in the laboratory of Shandong University, China. Sandstone and gneiss blocks were first to present Schmidt hammer test. Cores were then drilled from blocks, which were used to perform the P-wave velocity test. To ensure a high degree of correlation, specimens of Brazilian test and point load test were cut from the same core. Figure 3 shows the

Table 2 Results of laboratory experiments on sandstone and corresponding STD and COV

No.	Sample type	Brazilian strength BTS		Point load index $I_{s(50)}$		P-wave velocity V_P		Schmidt hardness R	
		Magnitude ± STD (MPa)	COV (%)	Magnitude ± STD (MPa)	COV (%)	Magnitude ± STD (m/s)	COV (%)	Magnitude ± STD	COV (%)
A	Fine grain size	3.94 ± 0.81	20.56	5.45 ± 0.73	13.39	3137 ± 358.69	11.43	37.0 ± 2.38	6.43
B		5.61± 0.10	1.78	6.08 ± 0.07	1.15	3442 ± 31.18	0.91	41.4 ± 0.66	1.61
C		6.99 ± 1.67	23.89	6.23 ± 0.12	1.93	3228 ± 137.08	4.25	37.0 ± 1.29	3.49
D		6.22 ± 1.58	25.40	6.80 ± 0.26	3.82	2953 ± 25.74	0.87	37.5 ± 2.23	5.95
E		11.07 ± 1.64	14.81	10.31 ± 0.13	1.26	3761 ± 151.37	4.02	57.0 ± 2.13	3.74
F		7.41 ± 2.19	29.55	7.56 ± 0.50	6.79	3819 ± 331.45	8.68	49.5 ± 1.27	2.57
G		4.06 ± 0.80	19.70	6.02 ± 0.62	10.30	2844 ± 21.18	0.74	39.5 ± 1.85	4.68
H	Coarse grain size	4.93 ± 1.04	21.10	7.08 ± 1.19	16.81	3531 ± 1.00	0.03	38.0 ± 3.38	8.89
I		3.09 ± 1.09	35.28	4.96 ± 0.06	1.21	3526 ± 10.50	0.30	39.0 ± 2.78	7.13
J		3.63 ± 0.92	25.34	7.93 ± 0.16	2.02	3881 ± 148.26	3.82	37.0 ± 2.38	6.43
K		3.26 ± 0.64	19.63	6.08 ± 1.73	28.45	4108 ± 318.55	7.75	42.0 ± 3.26	7.76
L		2.49 ± 0.42	16.87	1.97 ± 0.03	1.52	2375 ± 111.40	4.69	35.6 ± 3.28	9.21
M		3.43 ± 0.88	25.66	4.13 ± 0.77	18.64	3200 ± 106.17	3.32	23.0 ± 0.53	2.30
N		3.75 ± 0.78	20.80	2.51 ± 0.66	26.29	3511 ± 44.43	1.27	37.0 ± 1.94	5.24

Note: *STD* Standard Deviation, *COV* coefficient of variation

experimental set-up and representative failure modes of samples. The experiment results of tested samples are listed in Table 2-3.

The Brazilian test was presented following the method of China National Standard (2013). The core samples have a diameter of 50 mm and height to diameter ratio of 1.0. To produce uniform tensile stress distribution, core samples were clamped by two steel loading jaws which contact cylinder samples at diametrically-opposed surfaces (Fig. 3(a)). Samples were then compressed with a capacity of 2000 kN until failure. Rock specimens fail in typical tensile splitting failure mode (Fig. 3(b)). The final BTS (MPa) was obtained by averaging at least three specimens. This study used ten specimens due to their strong anisotropic properties.

The point load test was performed following the China National Standard (2013). The test was conducted on samples with a diameter (D) of 50 mm and height-to-diameter ratio of 0.5-1.0 (Fig. 3(c)). A steady load was applied on the specimens until failure, and several brittle fractures were always observed around the concentrated loading points (Fig. 3(d)). The test was repeated at least five times (ten times in study) to calculate the $I_{s(50)}$ (MPa).

Ultrasonic pulse velocity test following the China National Standard (2013) as well. P-wave velocity (V_p) was measured using a Portable Ultrasonic Non-destructive Digital Indicating Tester (pulse 54 kHz) (Fig. 3(e)). Grease was used to achieve an acceptable acoustic coupling between the transducers and samples. The transit time was measured to calculate the V_p (m/s).

Due to the high strength and hardness of the rock samples, the Schmidt hammer test was conducted on rock blocks using N-type hammer following the ISRM (2015) recommendation. The hammer possesses impact energies of 2.207 N m. Rock blocks were cut by saw and later smoothed using fine sandpaper. The hammer impact direction remains perpendicular to the flat rock surfaces and

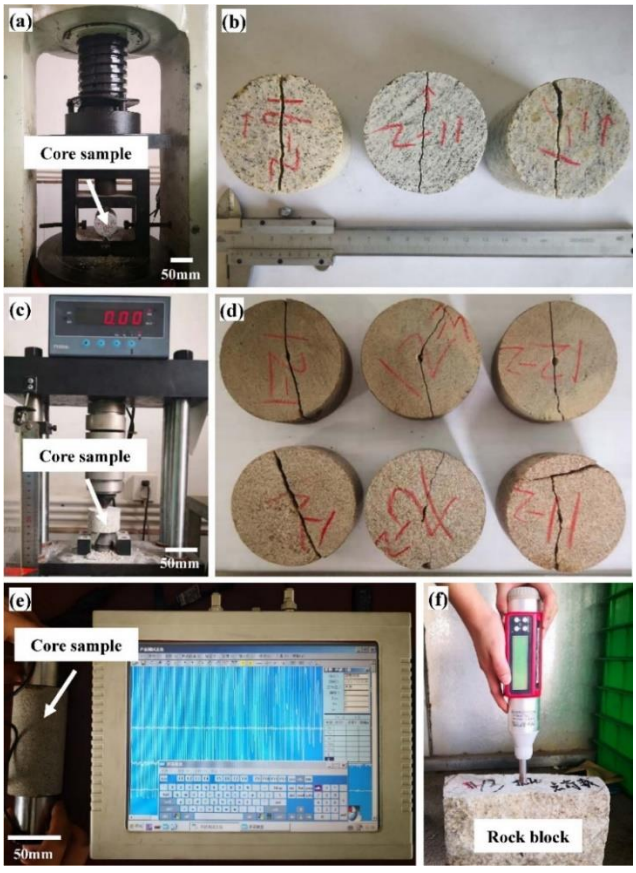

Fig. 3 Experimental setup and sample failure modes of different test types. (a)-(b) Brazilian test; (c)-(d) point load test.; (e) P-wave velocity test; (f) Schmidt hammer test

Table 3 Results of laboratory experiments on gneiss and corresponding STD and COV

No.	Sample type	Brazilian strength BTS Magnitude ± STD (MPa)	COV (%)	Point load index $I_{s(50)}$ Magnitude ± STD (MPa)	COV (%)	P-wave velocity V_P Magnitude ± STD (m/s)	COV (%)	Schmidt hardness R Magnitude ± STD	COV (%)
A	β = 0°	3.98 ± 1.66	41.71	2.42 ± 0.32	13.22	2851 ± 139.16	4.88	57.0 ± 0.99	1.74
B		4.75 ± 0.75	15.79	8.68 ± 0.47	5.41	3716 ± 81.08	2.18	58.5 ± 0.75	1.28
C		5.47 ± 1.41	25.78	6.35 ± 0.86	13.56	4700 ± 8.97	0.19	55.0 ± 1.78	3.24
D		5.02 ± 1.76	35.06	5.76 ± 0.57	9.90	4849 ± 75.66	1.56	49.5 ± 1.53	3.09
E		2.56 ± 0.37	14.45	0.76 ± 0.16	21.05	2544 ± 0.50	0.02	33.0 ± 1.43	4.33
F		4.94 ± 0.94	19.03	3.86 ± 0.39	10.10	3286 ± 118.75	3.61	49.0 ± 0.38	0.78
G	β = 45°	3.74 ± 0.65	17.38	4.59 ± 1.24	27.02	3265 ± 67.33	2.06	61.5 ± 0.75	1.22
H		2.23 ± 0.62	27.80	2.36 ± 1.06	44.92	2517 ± 73.28	2.91	36.5 ± 0.95	2.60
I		2.45 ± 0.31	12.65	4.04 ± 0.76	18.81	3479 ± 102.39	2.94	54.9 ± 1.89	3.44
J		3.46 ± 0.25	7.23	4.96 ± 1.02	20.56	3713 ± 109.54	2.95	57.5 ± 1.79	3.11
K		1.91 ± 0.03	1.57	2.27 ± 0.16	7.05	2261 ± 3.50	0.15	49.5 ± 0.75	1.52
L		3.09 ± 0.28	9.06	3.02 ± 0.41	13.58	2104 ± 67.38	3.20	55.0 ± 0.86	1.56
M	β = 90°	4.03 ± 0.43	10.67	5.21 ± 0.37	7.10	3597 ± 61.90	1.72	60.3 ± 0.47	0.78
N		1.41 ± 0.28	19.86	2.82 ± 0.46	16.31	2428 ± 77.85	3.21	55.0 ± 0.95	1.73
O		3.43 ± 0.19	5.54	4.57 ± 0.65	14.22	3621 ± 132.50	3.66	62.0 ± 0.93	1.50
P		1.72 ± 0.11	6.40	2.23 ± 0.18	8.07	2378 ± 78.85	3.32	58.5 ± 0.85	1.45
Q		4.35 ± 0.41	9.43	5.74 ± 0.83	14.46	3458 ± 84.53	2.44	53.5 ± 1.55	2.90
R		2.34 ± 0.12	5.13	3.71 ± 0.43	11.59	3158 ± 86.51	2.74	61.0 ± 0.81	1.33
S		2.69 ± 0.35	13.01	2.96 ± 0.65	21.96	3257 ± 2.00	0.06	45.6 ± 1.69	3.71

Note: *STD* Standard Deviation, *COV* coefficient of variation

Table 4 Results of regression analyses and corresponding parameters

Test types	Samples	Equations	No.	R^2	*P*-value	AIC	PI
Point load	Fine grain size	$BTS=1.407I_{s(50)}-3.223$	(1)	0.89	1.50×10^{-3}	-1.96	88.82
	Coarse grain size	$BTS=0.186I_{s(50)}+2.594$	(2)	0.31	1.95×10^{-1}*	-	-
	All sandstone samples	$BTS=0.810I_{s(50)}+1.934$	(3)	0.56	2.05×10^{-3}	25.08	-6.77
	β = 0°	$BTS=2.967I_{s(50)}^{0.293}$	(4)	0.87	1.14×10^{-4}	-7.76	78.80
	β = 45°	$BTS=1.248I_{s(50)}^{0.644}$	(5)	0.68	4.64×10^{-4}	-9.41	66.32
	β = 90°	$BTS=0.804I_{s(50)}-0.277$	(6)	0.89	1.57×10^{-3}	-12.58	89.05
	All gneiss samples	$BTS=0.476I_{s(50)}+1.436$	(7)	0.53	4.24×10^{-4}	-5.94	52.51
P-wave velocity	Fine grain size	$BTS=0.0047V_p-9.089$	(8)	0.54	1.55×10^{-3}	9.21	43.30
	Coarse grain size	$BTS=0.0157V_P^{0.663}$	(9)	0.32	2.77×10^{-4}	-4.67	19.58
	All sandstone samples	$BTS=0.0035V_P^{0.885}$	(10)	0.10	9.16×10^{-5}	23.71	2.69
	β = 0°	$BTS=3.417\ln(V_p)-23.487$	(11)	0.73	2.09×10^{-4}	-6.39	73.20
	β = 45°	$BTS=1.556e^{0.0002V_P}$	(12)	0.25	-*	-	-
	β = 90°	$BTS=0.244e^{0.0008V_P}$	(13)	0.88	1.21×10^{-4}	-5.88	70.36
	All gneiss samples	$BTS=0.0012V_p-0.611$	(14)	0.59	1.22×10^{-4}	-8.32	57.17
Schmidt hammer	Fine grain size	$BTS=0.264R-4.805$	(15)	0.70	1.82×10^{-2}	4.80	69.82
	Coarse grain size	$BTS=0.341R^{0.649}$	(16)	0.38	2.32×10^{-4}	-5.23	25.80
	All sandstone samples	$BTS=0.242R-4.509$	(17)	0.62	8.59×10^{-4}	10.94	60.97
	β = 0°	$BTS=0.066R^{1.074}$	(18)	0.67	6.01×10^{-4}	-2.89	51.40
	β = 45°	$BTS=0.868e^{0.0219R}$	(19)	0.52	5.76×10^{-4}	-8.32	59.46
	β = 90°	$BTS=0.0127R+2.136$	(20)	0.004	8.90×10^{-1}*	-	-
	All gneiss samples	$BTS=1.485\ln(R)-2.54$	(21)	0.06	1.67×10^{-7}	7.48	3.19

Note: **P*-value exceeds the upper limit and the equation is not significant. AIC and PI were not calculated for nonsignificant equations

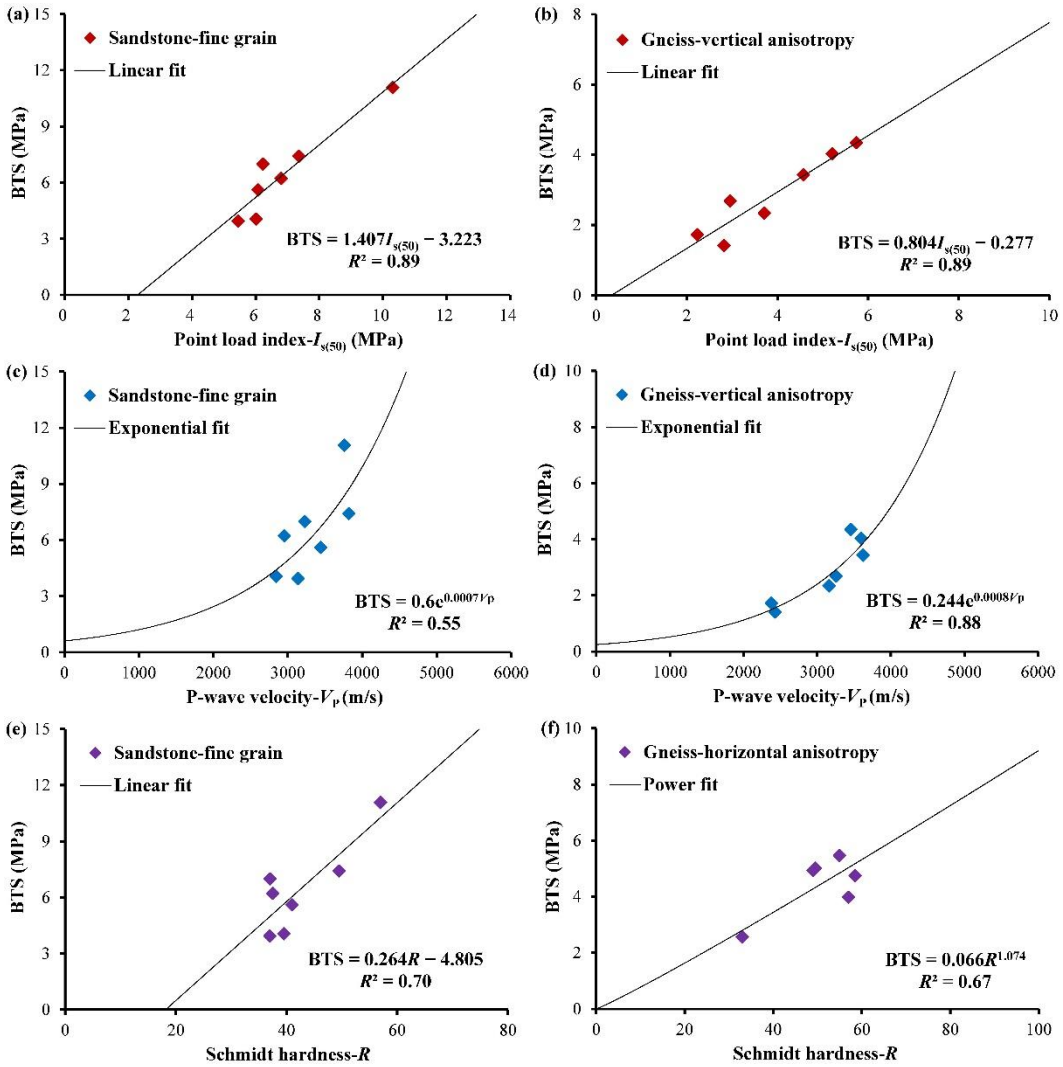

Fig. 4 Significant equations between BTS and index tests. (a) BTS-$I_{s(50)}$ of sandstone; (b) BTS-$I_{s(50)}$ of gneiss; (c) BTS-V_P of sandstone; (d) BTS-V_P of gneiss; (e) BTS-R of sandstone; (f) BTS-R of gneiss

a rebound value-R can be read directly on the device (Fig. 3(f)). Each impact position should be separated by at least a plunger diameter of the hammer. This procedure was repeated at least 20 times on each specimen to obtain the final R. The test may be stooped when 10 subsequent readings fluctuate in the repeatability range of ±2.

3. Regression analysis

Regression analysis was used to develop the correlations between BTS and each rock index property (i.e. $I_{s(50)}$, V_p and R). In the analysis, four function types including linear, power, exponential and logarithmic were examined for each type of sample, and the equation with the highest correlation coefficient-R^2 was considered as the best fitting equation. Moreover, the F-value and P-value (probability > F-value) were used to verify the significance of the proposed equation within the 95% confidence interval. Once the P-value is smaller than 0.05, the equation is significant and valid (OriginLab 2019).

Table 4 shows empirical equations for estimating BTS of sandstone and gneiss samples. It can be seen that several significant correlations were established, such as BTS-$I_{s(50)}$ of fine-grained sandstone, BTS-V_p of gneiss with β=90°, BTS-R of fine-grained sandstone, etc. But, correlations between BTS and index properties depend on grain size or anisotropy; and no acceptable statistical correlations can be derived from $I_{s(50)}$ of coarse-grained sandstone, V_p of gneiss with β=45° and R of gneiss with β=90°. Figs. 4(a)-(f) shows the most significant equation of BTS-$I_{s(50)}$, BTS-V_p and BTS-R for sandstone or gneiss, respectively.

4. Results verification, comparison and discussion

4.1 Impact of grain size or anisotropy on experiment results

To assess the impact of grain size or anisotropy on the laboratory experiment results, the coefficient of variation (COV) was calculated for each test data. The COV is

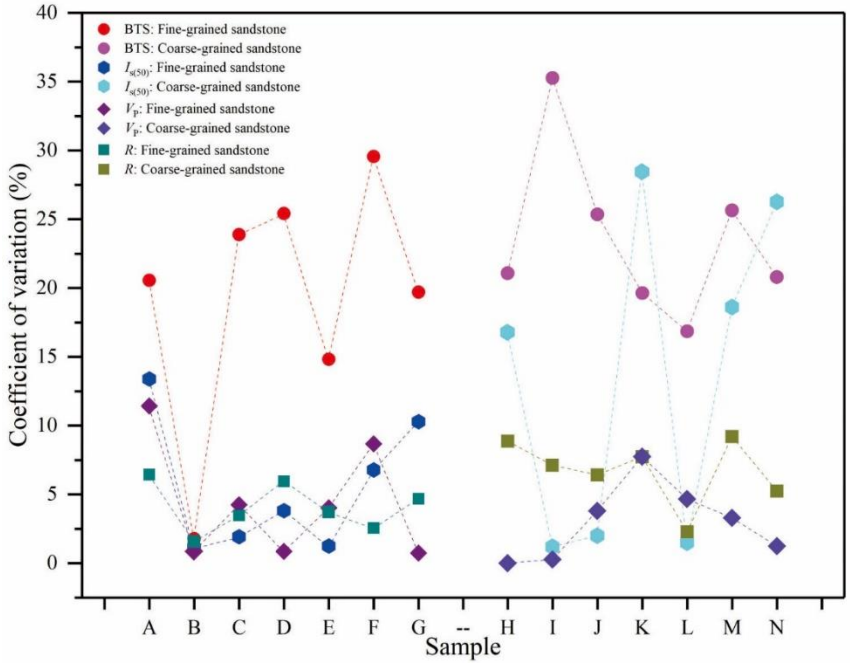

Fig. 5 The coefficient of variation of laboratory experiment data for sandstone

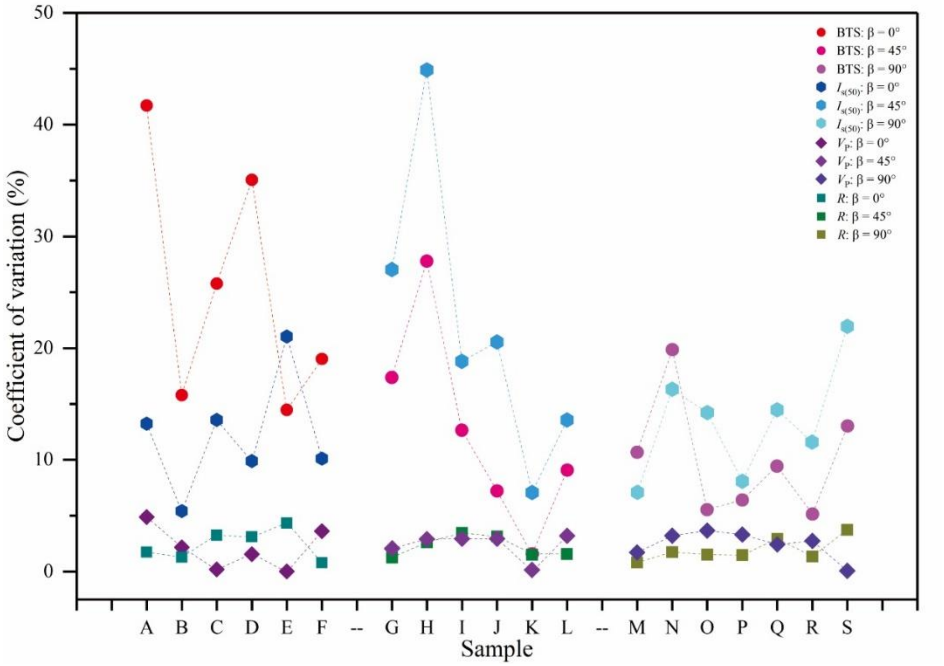

Fig. 6 The coefficient of variation of laboratory experiment data for gneiss

defined as the ratio of the standard deviation to the mean value and can reflect the discreteness characteristics. All the calculated COVs are listed in Table 2-3. Also, Figs. 5 and 6 compare the COVs derived from different types of samples.

As seen in Fig. 5, grain size variation exerts absolute control on the discreteness of BTS, where the COV values increase markedly when the grain size shift from fine (COVs from 1.78% to 29.55%) to coarse (COVs between 16.87% to 35.28%). Also, increasing grain size is a crucial factor to consider for the point load and Schmidt hammer test. For example, the $I_{s(50)}$ of coarse-grained sandstone display a wider fluctuating range of COVs than those data of fine-grained sandstone, where COVs ranging from 1.21% to 28.45%. Similarly, a larger magnitude of COVs can be observed from the Schmidt hardness of coarse-grained sandstone (COVs between 2.30% to 9.21%). The discreteness of P-wave velocities, but, exhibit different changing tendencies following increasing grain size, which can be demonstrated by the negligible changes in COVs (Fig. 5).

As shown in Fig. 6, the discreteness of BTS data declines continuously along with the increasing anisotropy inclination (i.e. β from 0°, through 45° to 90°), reflected by the decrease of COVs. For the point load index, the

differences of COVs are negligible for samples with horizontal and vertical anisotropy, but peaked sharply when test applied at β=45° (COVs from 7.05% to 44.92%). Moreover, the inconsiderable impact of anisotropy orientation on P-wave velocity and Schmidt hardness can be observed, where COVs have a steady fluctuating range following changing anisotropy orientations (Fig. 6).

4.2 Role of grain size or anisotropy on the regression analysis parameters

Apart from the correlation coefficients (R^2), statistics indices including Akaike Information Criterion (AIC) and performance index (PI) were calculated for the proposed equations of this study (see Table 4). The equation, which has the smallest value of AIC and the biggest value of PI, will exhibit the best performance in the BTS estimation.

$$\mathrm{AIC} = N \ln\left[\sum_{i=1}^{N} \frac{(\mathrm{y} - \mathrm{y}')^2}{N}\right] + 2n_{\mathrm{P}} \tag{22}$$

where N is the total number of samples; y is measured BTS; y' is calculated BTS; n_{p} is the number of parameters that must be estimated.

$$\mathrm{PI} = \left[\mathrm{COD} + \left(\frac{\mathrm{VAF}}{100}\right) - \mathrm{RMSE}\right] \tag{23}$$

where COD is the coefficients of determination; VAF is the variance accounts for (%); RMSE is the root-mean-square error.

The value of COD, VAF and RMSE can be calculated as the following equations:

$$\mathrm{COD} = 1 - \frac{\sum (y - y')^2}{\sum (y - \bar{y})^2} \tag{24}$$

$$\mathrm{VAF} = \left[1 - \frac{\mathrm{var}(y - y')}{\mathrm{var}(y)}\right] \times 100 \tag{25}$$

$$\mathrm{RMSE} = \sqrt{\frac{1}{n}\sum_{i=1}^{N} (y - y')^2} \tag{26}$$

Where $\bar{y}$ is the mean value of measured BTS; var is variance; n is the degree of freedom (referred to N minus 1).

As shown in Table 4, the correlations of BTS-$I_{s(50)}$ are dramatically dominated by the grain size, varying in the slope and intercept of equations. Further, the equation of BTS-$I_{s(50)}$ through fine-grained sandstone has the smallest value of AIC and the highest value of R^2 and PI, which indicates the best performance for predicting BTS. However, no significant correlation can be expected from $I_{s(50)}$ to estimate BTS of coarse-grained sandstone. Compared with fine-grained samples, the correlation degree between BTS and $I_{s(50)}$ (Eq. (3)) decays noticeably when samples contain noticeable grain size variation (R^2 ranging from 0.89 to 0.56).

Moreover, the anisotropy orientation plays an important role in the function types of empirical equations, reflected by the various power and linear functions (Eqs. 4-7). The equation of BTS-$I_{s(50)}$ via samples with β=90° has the highest R^2, PI value and smallest AIC value. Conversely, the BTS and $I_{s(50)}$ from test at β=45° exhibits the most inferior degree of correlation. Moreover, multi-directional anisotropies can exert negative impacts on the equation of BTS-$I_{s(50)}$, reducing the correlation degree between BTS and $I_{s(50)}$ (Eq. (7)), probably provoking considerable error for estimated BTS.

For the P-wave velocity, an inferior degree of correlation between BTS-V_{p} can be observed from sandstone samples, where the biggest R^2 value only reaches up to 0.54. The P-wave velocity is not reliable to estimate BTS of sandstones used in this study and should be used with much care, although this index property has been widely used to estimate BTS.

Anisotropy orientation is also an important role to consider for predicting BTS by V_{p}, where four function types (Eqs. 11-14) including logarithmic, exponential and linear can be seen through samples with different anisotropy inclination. No significant correlation of BTS-V_{p} can be derived for the test at β=45°, reflected by an R^2 value of 0.25. Moreover, the highest R^2 (0.88) can be seen from the equation of samples with β=90° while the best performance of PI (73.20) emerges in the formula of samples with β=0°. Compared with unidirectional anisotropy, the multi-directional anisotropies lead to a decline in the degree of correlation between BTS and V_{p} (Eq. (14)).

For the Schmidt hammer test, the functions of the proposed formulas (i.e. linear, power, exponential and logarithmic; Eqs 15-21) are guided by the grain size or anisotropy. The R^2 value of the equation between BTS and R decreases sharply when the grain size shift from fine to coarse, ranging from 0.70 to 0.38. Meanwhile, the AIC and PI performances also exhibit a corresponding fluctuating tendency.

Moreover, anisotropy inclination perturbs the degree of correlation between BTS and R, where nonsignificant equation can be developed for the test at β=90°. Interestingly, although the R^2 value of samples with β=0° is bigger than samples β=45°, the performances of AIC and PI present the opposite case. Also, multi-directional anisotropies display negative impacts on the regression performance of the equation of BTS-R (Eq. (21)), reflected by the biggest value of AIC and the smallest value of R^2 and PI.

4.3 Impact of grain size or anisotropy on the estimation capability of the equation

In this study, to reflect the impact of grain size or anisotropy on the estimation capability of derived equations, the relative error (RE) and mean absolute percentage error (MAPE) of estimated BTS were calculated by the following formulas.

$$\mathrm{RE} = \left(\frac{y - y'}{y}\right) \times 100 \tag{27}$$

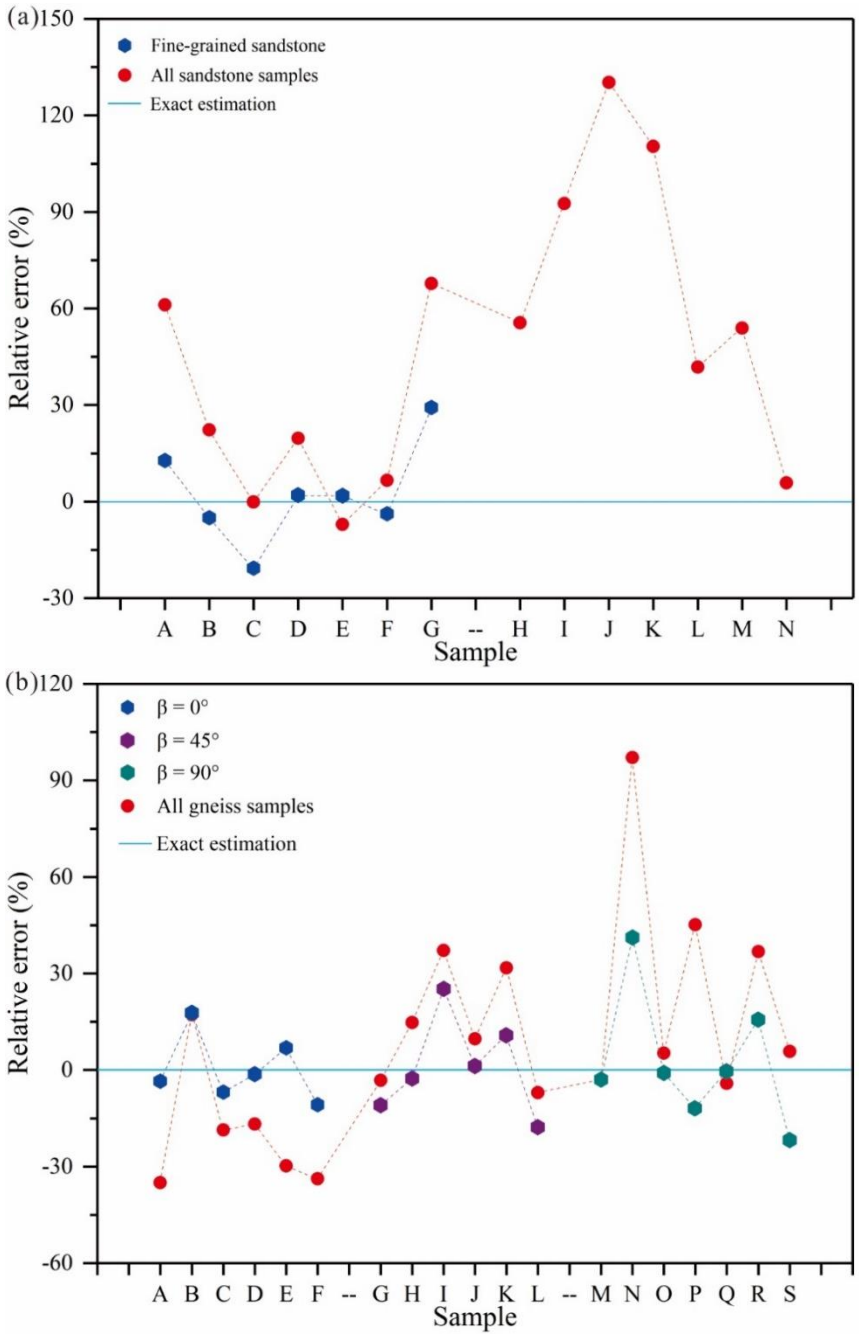

Fig. 7 The relative errors of estimated BTS through point load index. (a) sandstone samples; (b) gneiss samples

$$\text{MAPE} = \frac{1}{N}\sum_{i=1}^{N}\left|\frac{(y\text{-}y')}{y}\right| \times 100 \quad (28)$$

where y is measured BTS; y' is calculated BTS; N is the total number of samples.

Tables 5-9 list the calculated RE and MAPE values and the fluctuating tendencies of RE are also depicted in Figs. 7-9. The RE and MAPE were not calculated and shown for nonsignificant equations (P-value more than 0.05).

For the point load test, considerable RE magnitudes can be seen from the estimated BTS of samples containing significant grain size variation, with a maximum overestimation of 130.23% and a maximum underestimation of up to 7.09% (Fig. 7(a)). Subsequently, the RE and MAPE magnitudes weaken substantially when the estimated BTS is derived from fine-grained samples, where the RE fluctuates between -20.71% and 29.24% while MAPE drops to 15.57% (Table 5).

The RE data points of estimated BTS through samples with β=0° cluster uniformly around the exact estimation lines, with an acceptable deviation of ~ ±20% (Eq. (4)). Huge differences can be seen from the regression analysis performance of two equations (Eqs. 5 and 6) through samples with β=45° or 90°, but, these equations exhibit similar reliability in the BTS estimation, reflected by similar RE fluctuating range and MAPE value. Once the samples contain different anisotropy orientations (Eq. (7)),

Table 5 The relative errors of estimated BTS via $I_{s(50)}$ of sandstone

Sample	Measured BTS (MPa)	Estimated BTS using Eq. (1)			Estimated BTS using Eq. (3)		
		Value (MPa)	RE (%)	MAPE (%)	Value (MPa)	RE (%)	MAPE (%)
A	3.94	4.45	12.82		6.35	61.13	
B	5.61	5.33	-4.96		6.86	22.26	
C	6.99	5.54	-20.71		6.98	-0.14	
D	6.22	6.34	2.00	15.57	7.44	19.65	
E	11.07	11.28	1.93		10.29	-7.09	
F	7.41	7.13	-3.74		7.90	6.55	
G	4.06	5.25	29.24		6.81	67.74	42.65
H	4.93	-	-	-	7.67	55.55	
I	3.09	-	-	-	5.95	92.61	
J	3.63	-	-	-	8.36	130.23	
K	3.26	-	-	-	6.86	110.39	
L	2.49	-	-	-	3.53	41.76	
M	3.43	-	-	-	5.28	53.92	
N	3.75	-	-	-	3.97	5.79	

Table 6 The relative errors of estimated BTS via $I_{s(50)}$ of gneiss

No.	Measu-red BTS (MPa)	Estimated BTS by Eq. (4)			Estimated BTS by Eq. (5)			Estimated BTS by Eq. (6)			Estimated BTS by Eq. (7)		
		Value (MPa)	RE (%)	MAPE (%)	Value (MPa)	RE (%)	MAPE (%)	Value (MPa)	RE (%)	MAPE (%)	Value (MPa)	RE (%)	MAPE (%)
A	3.98	3.84	-3.42					-	-	-	2.59	-34.98	
B	4.75	5.59	17.65					-	-	-	5.57	17.21	
C	5.47	5.10	-6.82	7.82				-	-	-	4.45	-18.58	
D	5.02	4.96	-1.28					-	-	-	4.18	-16.78	
E	2.56	2.74	6.94					-	-	-	1.80	-29.78	
F	4.94	4.41	-10.78					-	-	-	3.27	-33.74	
G	3.74	-	-	-	3.33	-10.97					3.62	-3.19	
H	2.23	-	-	-	2.17	-2.71					2.56	14.77	
I	2.45	-	-	-	3.07	25.19	11.42				3.36	37.10	
J	3.46	-	-	-	3.50	1.16					3.80	9.74	23.78
K	1.91	-	-	-	2.12	10.78					2.52	31.75	
L	3.09	-	-	-	2.54	-17.70					2.87	-7.01	
M	4.03	-	-	-	-	-	-	3.91	-2.93		3.92	-2.83	
N	1.41	-	-	-	-	-	-	1.99	41.15		2.78	97.04	
O	3.43	-	-	-	-	-	-	3.40	-0.95		3.61	5.29	
P	1.72	-	-	-	-	-	-	1.52	-11.87	13.52	2.50	45.20	
Q	4.35	-	-	-	-	-	-	4.34	-0.28		4.17	-4.18	
R	2.34	-	-	-	-	-	-	2.71	15.63		3.20	36.84	
S	2.69	-	-	-	-	-	-	2.10	-21.83		2.84	5.76	

the RE and MAPE of estimated BTS grow dramatically, where the RE change between -34.98% and 97.04% while the MAPE reaches 23.78% (Fig. 7(b), Table 6).

It was noted that no reliable correlations can be derived from V_P to estimate BTS of sandstone samples in this study, with R^2 value smaller than 0.54. Similar to the point load test, rocks with significant grain size variation exhibit inferior reliability for estimating BTS using V_P, with the RE range between -53.86 and 69.40 (Fig. 8(a), Table 7). For the P-wave velocity through gneiss samples, equation from the test at β=0° (Eq. (11)) exhibits the highest reliability in the BTS estimation, reflected by the narrowest fluctuating

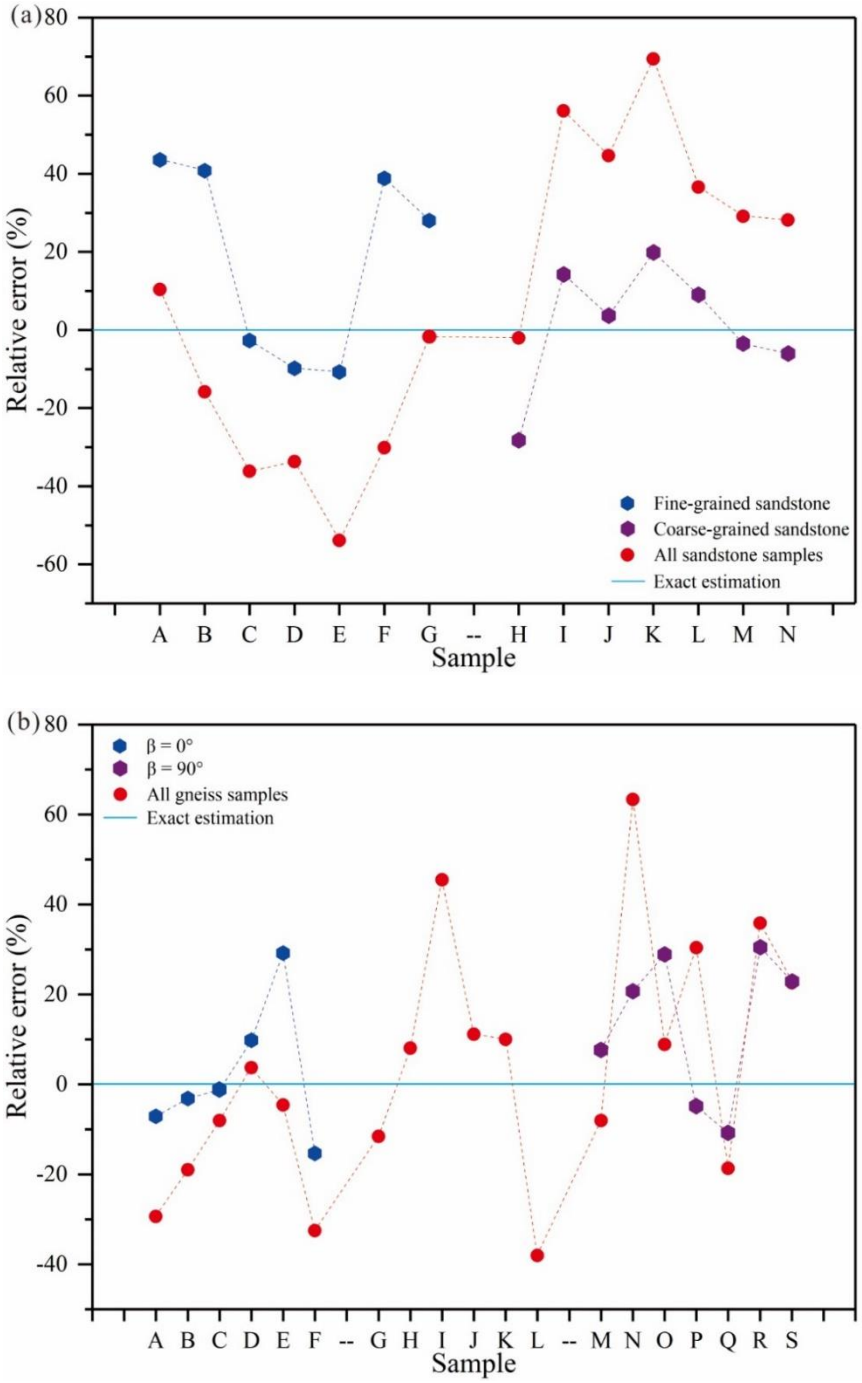

Fig. 8 The relative errors of estimated BTS through P-wave velocity. (a) sandstone samples; (b) gneiss samples

range of RE (from -15.35% to 29.19%) and smallest MAPE value of 10.96 (Fig. 8(b), Table 8). Moreover, considerable discrepancies can be observed between the estimated BTS and the measured values derived from samples with multidirectional anisotropy (Eq. (14)), with a maximum overestimation of up to 63.50% and a maximum underestimation of 38.06%.

The impact of grain size on the BTS-*R* equations was quite similar to the BTS- V_P equations, reflected by a similar fluctuating tendency of RE values (Fig. 9(a), Table 9). Moreover, the samples with grain size variation are less reliable for calculating BTS; and the maximum positive and negative RE can be up to 59.51% and -57.55%, respectively.

Corresponding to the similar performance of regression analysis, similar BTS estimation capability can be observed between test at β=0° and β=45°, which can be verified by the similar RE fluctuating range and MAPE value (Fig. 9(b), Table 10). However, the deviation of estimated BTS increases dramatically when Schmidt hardness from samples with three anisotropy orientations, reflected by the wider range of RE (between -37.64% and 141.91%) and higher MAPE value of 34.41.

Table 7 The relative errors of estimated BTS via V_P of sandstone

No.	Measured BTS (MPa)	Estimated BTS using Eq. (8)			Estimated BTS using Eq. (9)			Estimated BTS using Eq. (10)		
		Value (MPa)	RE (%)	MAPE (%)	Value (MPa)	RE (%)	MAPE (%)	Value (MPa)	RE (%)	MAPE (%)
A	3.94	5.65	43.53		-	-	-	4.35	10.40	
B	5.61	7.90	40.83		-	-	-	4.72	-15.83	
C	6.99	6.80	-2.70		-	-	-	4.46	-36.17	
D	6.22	5.61	-9.80	24.96	-	-	-	4.12	-33.71	
E	11.07	9.88	-10.78		-	-	-	5.11	-53.86	
F	7.41	10.29	38.85		-	-	-	5.18	-30.13	
G	4.06	5.20	28.03		-	-	-	3.99	-1.76	31.99
H	4.93	-	-	-	3.53	-28.33		4.83	-2.03	
I	3.09	-	-	-	3.53	14.22		4.82	56.10	
J	3.63	-	-	-	3.76	3.62		5.25	44.67	
K	3.26	-	-	-	3.91	19.82	12.10	5.52	69.40	
L	2.49	-	-	-	2.72	9.09		3.40	36.56	
M	3.43	-	-	-	3.31	-3.50		4.43	29.07	
N	3.75	-	-	-	3.52	-6.14		4.81	28.16	

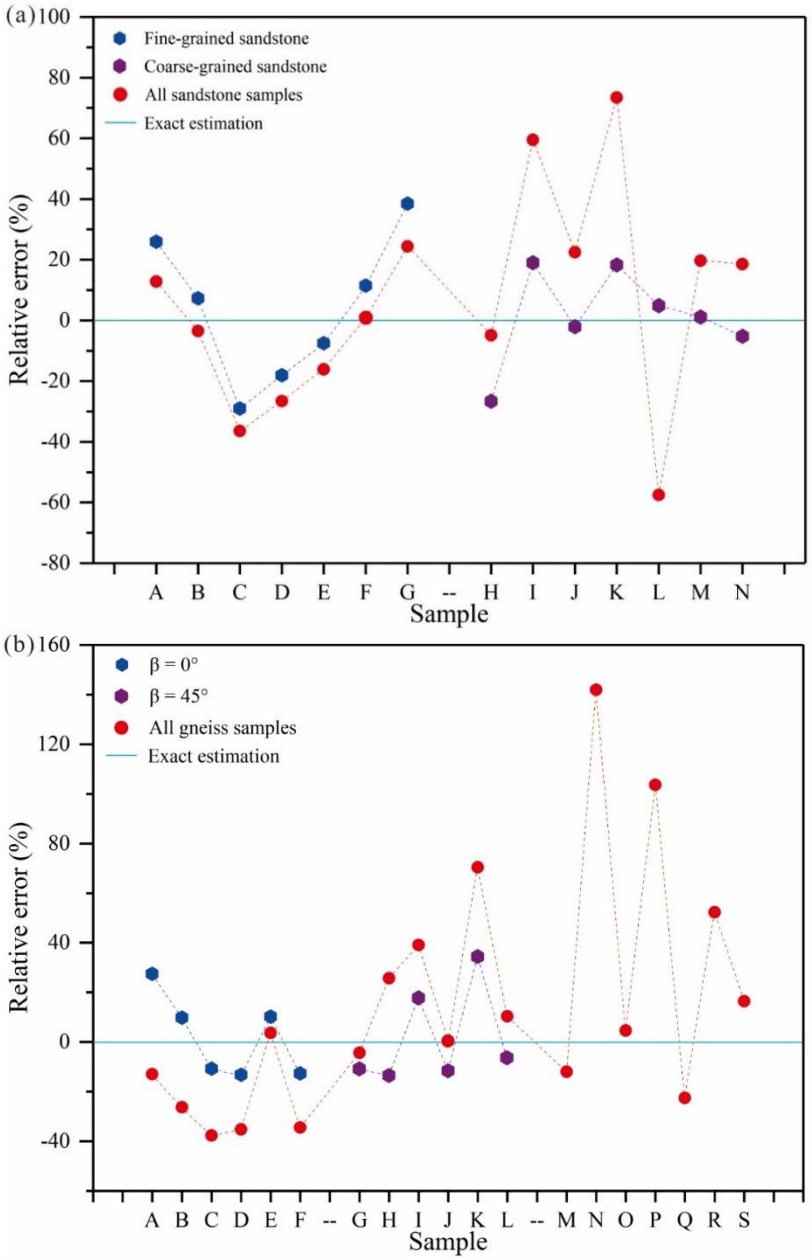

Fig. 9 The relative errors of estimated BTS using Schmidt hardness. (a) sandstone samples; (b) gneiss samples

Table 8 The relative errors of estimated BTS via V_P of gneiss

No.	Measu-red BTS (MPa)	Estimated BTS by Eq. (11)			Estimated BTS by Eq. (13)			Estimated BTS by Eq. (14)		
		Value (MPa)	RE (%)	MAPE (%)	Value (MPa)	RE (%)	MAPE (%)	Value (MPa)	RE (%)	MAPE (%)
A	3.98	3.70	-7.12		-	-	-	2.81	-29.39	
B	4.75	4.60	-3.11		-	-	-	3.85	-18.99	
C	5.47	5.40	-1.19	10.96	-	-	-	5.03	-8.06	
D	5.02	5.51	9.79		-	-	-	5.21	3.74	
E	2.56	3.31	29.19		-	-	-	2.44	-4.62	
F	4.94	4.18	-15.35		-	-	-	3.33	-32.55	
G	3.74	-	-	-	-	-	-	3.31	-11.58	
H	2.23	-	-	-	-	-	-	2.41	8.04	
I	2.45	-	-	-	-	-	-	3.56	45.46	
J	3.46	-	-	-	-	-	-	3.84	11.12	21.54
K	1.91	-	-	-	-	-	-	2.10	10.03	
L	3.09	-	-	-	-	-	-	1.91	-38.06	
M	4.03	-	-	-	4.34	7.60		3.71	-8.05	
N	1.41	-	-	-	1.70	20.71		2.30	63.30	
O	3.43	-	-	-	4.42	28.87		3.73	8.87	
P	1.72	-	-	-	1.64	-4.93	18.02	2.24	30.38	
Q	4.35	-	-	-	3.88	-10.81		3.54	-18.65	
R	2.34	-	-	-	3.05	30.43		3.18	35.84	
S	2.69	-	-	-	3.30	22.81		3.30	22.58	

Table 9 The relative errors of estimated BTS via R of sandstone

No.	Measured BTS (MPa)	Estimated BTS by Eq. (15)			Estimated BTS by Eq. (16)			Estimated BTS by Eq. (17)		
		Value (MPa)	RE (%)	MAPE (%)	Value (MPa)	RE (%)	MAPE (%)	Value (MPa)	RE (%)	MAPE (%)
A	3.94	4.96	25.96		-	-	-	4.45	12.82	
B	5.61	6.02	7.29		-	-	-	5.41	-3.51	
C	6.99	4.96	-29.00		-	-	-	4.45	-36.41	
D	6.22	5.10	-18.09	23.97	-	-	-	4.57	-26.59	
E	11.07	10.24	-7.47		-	-	-	9.29	-16.12	
F	7.41	8.26	11.51		-	-	-	7.47	0.81	
G	4.06	5.62	38.50		-	-	-	5.05	24.38	35.13
H	4.93	-	-	-	3.61	-26.69		4.69	-4.93	
I	3.09	-	-	-	3.68	18.96		4.93	59.51	
J	3.63	-	-	-	3.55	-2.14		4.45	22.45	
K	3.26	-	-	-	3.86	18.31	11.02	5.66	73.47	
L	2.49	-	-	-	2.61	4.79		1.06	-57.55	
M	3.43	-	-	-	3.46	1.01		4.11	19.71	
N	3.75	-	-	-	3.55	-5.27		4.28	17.06	

4.4 Comparison with previous studies

To explore the differences in correlations due to different grain size or anisotropy characteristics, previous empirical equations were used to calculate BTS based on the rock index properties of this study. Figures 10-12 show the comparison between the measured BTS (black dots) and the calculated BTS. Each column group represents an individual empirical equation, and the scattered data point is the estimated BTS based on the rock index properties of each specimen. For the point load test, the proposed correlations of sandstones were compared to previous studies using relative homogeneous rocks while the correlations of gneiss were compared with previous equations via anisotropic rocks. As the limit number of previous equations, the proposed equations of BTS-V_P/R form sandstone or gneiss are respectively compared with all previous equations.

As shown in Figs. 10-12, the correlations between BTS and index properties are significantly different once rocks characterized by various grain size or anisotropy properties. Using an empirical equation ignoring grain size or anisotropy can yield considerable discrepancies between the measured BTS and the calculated values. Even though the same sandstone or gneiss samples in this study, variation grain size or anisotropy orientation can still generate considerable errors of estimated BTS.

Table 10 The relative errors of estimated BTS via *R* of gneiss

No.	Measu-red BTS (MPa)	Estimated BTS by Eq. (18)			Estimated BTS by Eq. (19)			Estimated BTS by Eq. (21)		
		Value (MPa)	RE (%)	MAPE (%)	Value (MPa)	RE (%)	MAPE (%)	Value (MPa)	RE (%)	MAPE (%)
A	3.98	5.07	27.49		-	-	-	3.46	-12.97	
B	4.75	5.22	9.84		-	-	-	3.50	-26.26	
C	5.47	4.88	-10.73	14.01	-	-	-	3.41	-37.64	
D	5.02	4.36	-13.13		-	-	-	3.25	-35.17	
E	2.56	2.82	10.20		-	-	-	2.65	3.61	
F	4.94	4.31	-12.69		-	-	-	3.24	-34.43	
G	3.74	-	-	-	-	-	-	3.58	-4.36	
H	2.23	-	-	-	-	-	-	2.80	25.65	
I	2.45	-	-	-	-	-	-	3.41	39.11	
J	3.46	-	-	-	-	-	-	3.48	0.49	34.41
K	1.91	-	-	-	-	-	-	3.25	70.39	
L	3.09	-	-	-	-	-	-	3.41	10.38	
M	4.03	-	-	-	3.34	-10.76		3.55	-11.97	
N	1.41	-	-	-	1.93	-13.43		3.41	141.91	
O	3.43	-	-	-	2.89	17.90		3.59	4.63	
P	1.72	-	-	-	3.06	-11.63	15.73	3.50	103.63	
Q	4.35	-	-	-	2.57	34.36		3.37	-22.53	
R	2.34	-	-	-	2.89	-6.32		3.56	52.34	
S	2.69	-	-	-	3.34	-10.76		3.13	16.45	

Especially, the maximum underestimation of BTS reaches up to 491.75% through the equation of BTS-$I_{s(50)}$ (Gurocak *et al.* 2012) (see Fig. 10(a)). Also, an unacceptable error of estimated BTS appeared from the equation of Fereidooni (2016), i.e., a negative BTS value of 0.17 MPa. Moreover, considerable discrepancies can be seen between the estimated BTS and the measured values when the equation of BTS-$I_{s(50)}$ ignoring anisotropic orientation, with a maximum overestimation of BTS up to 279.40% (from the equation of Mishra and Basu 2012) (see Fig. 10(b)).

Meanwhile, different grain size or anisotropic properties can result in considerable discrepancies between the measured BTS and estimated values via correlation of BTS-V_p, where the maximum overestimations of BTS can be up to 380.55% and 560.99%, respectively (data from Khandelwal and Singh (2009)) (see Figs. 11(a)-(b)). Similar phenomena can be observed from the correlations between BTS and *R*; and the equation of Karaman *et al.* (2015) can predict BTS with maximum overestimations of 129.67% (through *R* of sandstone) and 550.15% (via *R* of gneiss), respectively (see Figs. 12(a)-(b)).

5. Conclusions and recommendations

To enhance the reliability of rock index properties on anisotropic and heterogeneous rocks in BTS estimation, this study presents new insights into the respective impact of grain size or anisotropy on the correlations between BTS and index properties. The aim was achieved by presenting intensive laboratory experiments as well as regression analysis. The regression analysis parameters and estimation capability of each proposed correlation have been discussed through comparative study. The following points are concluded from this work.

Increasing grain size or inclined anisotropy (i.e. β=45°) give rise to more discrete point load strength; and reliable point load index can be obtained when the test applied on fine-grained sandstone or at β=0° or 90° for gneiss. Moreover, empirical equation based on point load strength of fine-grained sandstone shows high reliability in the BTS estimation, but, no significant correlation of BTS-$I_{s(50)}$ can be derived from coarse-grained sandstone. For the anisotropic rock, point load index at β=45° exhibits inferior correlated degree to BTS than those tests at β=0° or 90°. However, the two equations of BTS-$I_{s(50)}$ from gneiss with β=45° or 90° have similar estimation capability for calculating BTS.

For the P-wave velocity test, varying grain size or anisotropy inclination exerts a negligible impact on the discreteness of V_P data. However, no reliable empirical equation of BTS-V_P can be expected for both fine and coarse-grained sandstone in this study; and the correlated degree between BTS and V_P declines dramatically due to the coarse grain size. Moreover, the empirical equation of BTS-V_P from samples with β=0° reveals the best performance in the BTS estimation. Also, the P-wave velocity test at β=45° is not valid for the estimation of BTS.

Coarse grain size leads to an escalation of discreteness of Schmidt hammer readings, but this phenomenon cannot be seen from the inclined anisotropy. Also, the correlated

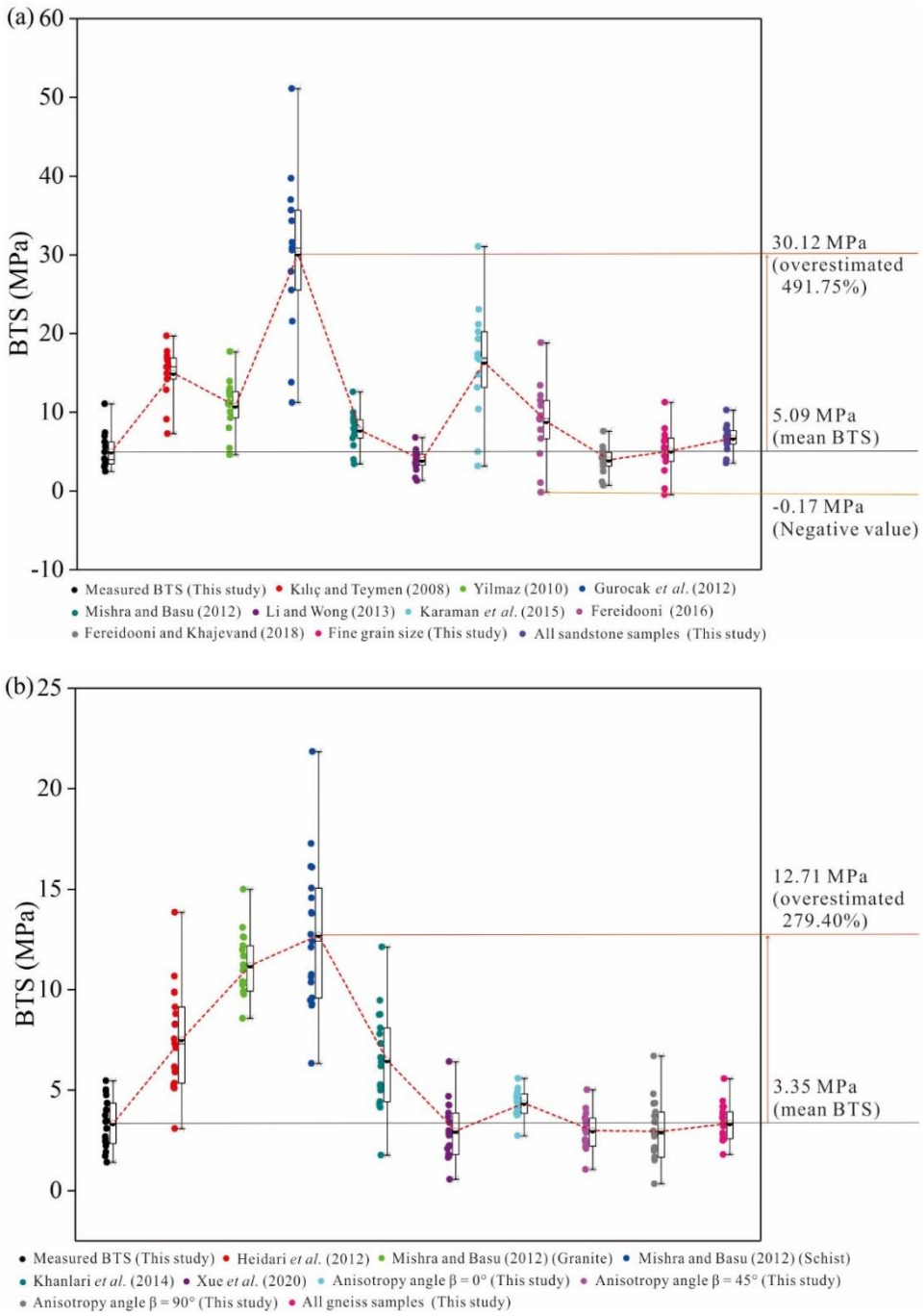

Fig. 10 Comparison between the proposed equations of BTS-$I_{s(50)}$ and previous studies. (a) sandstone samples; (b) gneiss samples

degree between BTS and *R* will weaken substantially by the impact of coarse grain size, where no reliable correlation of BTS-*R* can be derived. For the anisotropic rock, the Schmidt hammer tests performed at β=0° and β=45° show similar reliability in the BTS estimation. However, the empirical equation from samples with vertical anisotropy is not valid for predicting BTS; and a corresponding phenomenon can be seen from samples with multidirectional anisotropies.

The correlations between BTS and index properties are significantly different once rocks characterized by various grain size or anisotropy properties. Using an empirical equation ignoring grain size or anisotropy can yield considerable discrepancies between the measured BTS and the calculated values.

The present finding, thus, implies that either grain size variation or multidirectional anisotropy reduces not only the correlated degree between BTS and index tests, but also the BTS estimation reliability of those correlations. All three rock index properties should be used with much care for coarse-grained rocks; and should be respectively performed on samples with unidirectional anisotropy. Among three index properties, point load test is most reliable in the BTS estimation for both sandstone and gneiss, verified by the

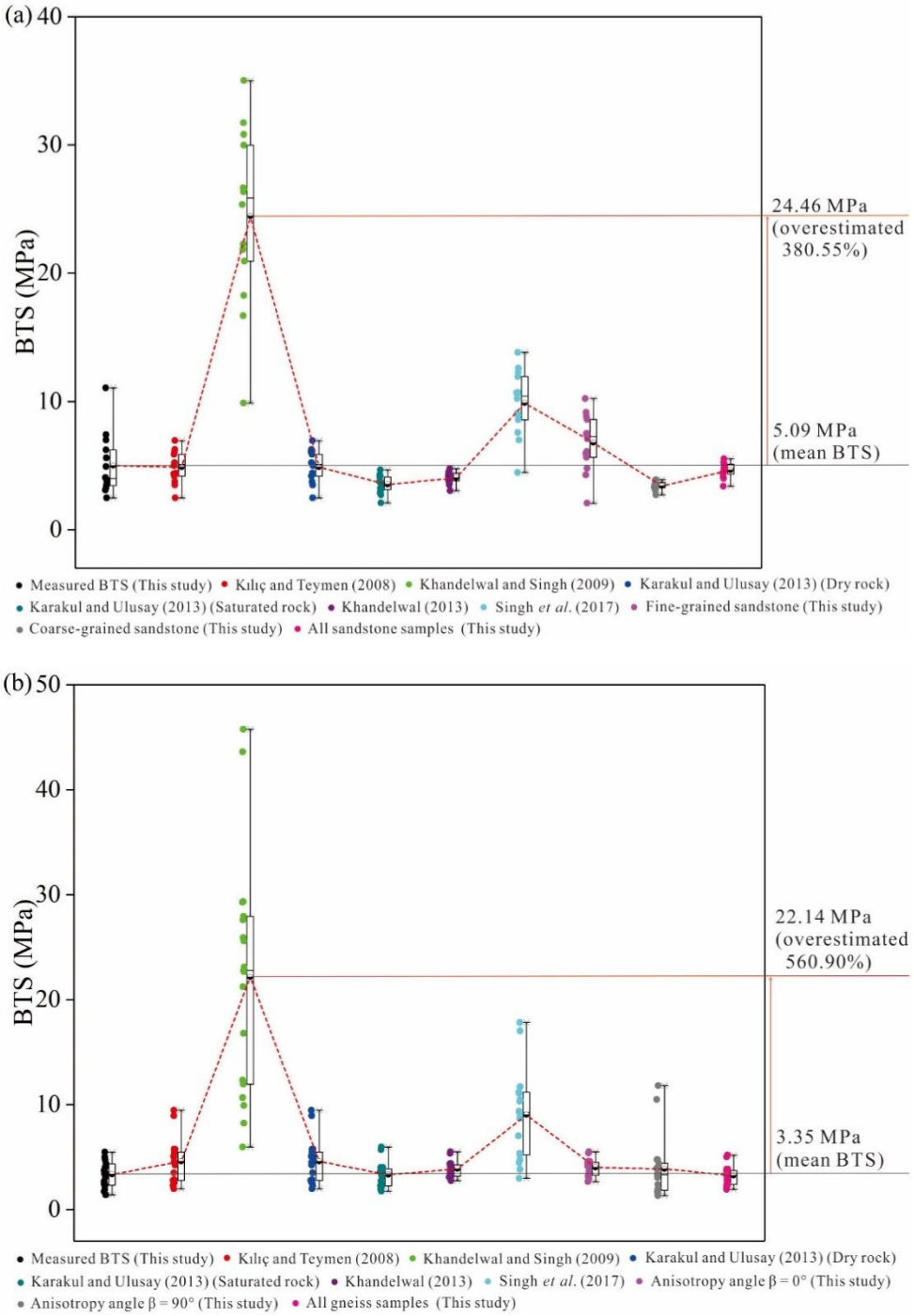

Fig. 11 Comparison between the proposed equations of BTS-V_P and previous studies. (a) sandstone samples; (b) gneiss samples

small discrepancies of estimated BTS. P-wave velocity test should not be performed at 45° angle to the anisotropy in the BTS estimation; and this recommendation is also appropriate for the Schmidt hammer test conducted parallel to anisotropy. Moreover, although developing empirical equations is not the main purpose of this study, the proposed equations can also be referenced by researchers and practitioners to estimate BTS for rocks with the same lithology, but with much care of grain size or anisotropy.

Acknowledgments

This work is financially supported by the National Natural Science Foundation of China (grant numbers 41877239, 41772298, 51379112, 51422904 and 40902084), and Fundamental Research Fund of Shandong University (grant number 2018JC044), and Shandong Provincial Natural Science Foundation (grant number 2019GSF111028 and JQ201513).

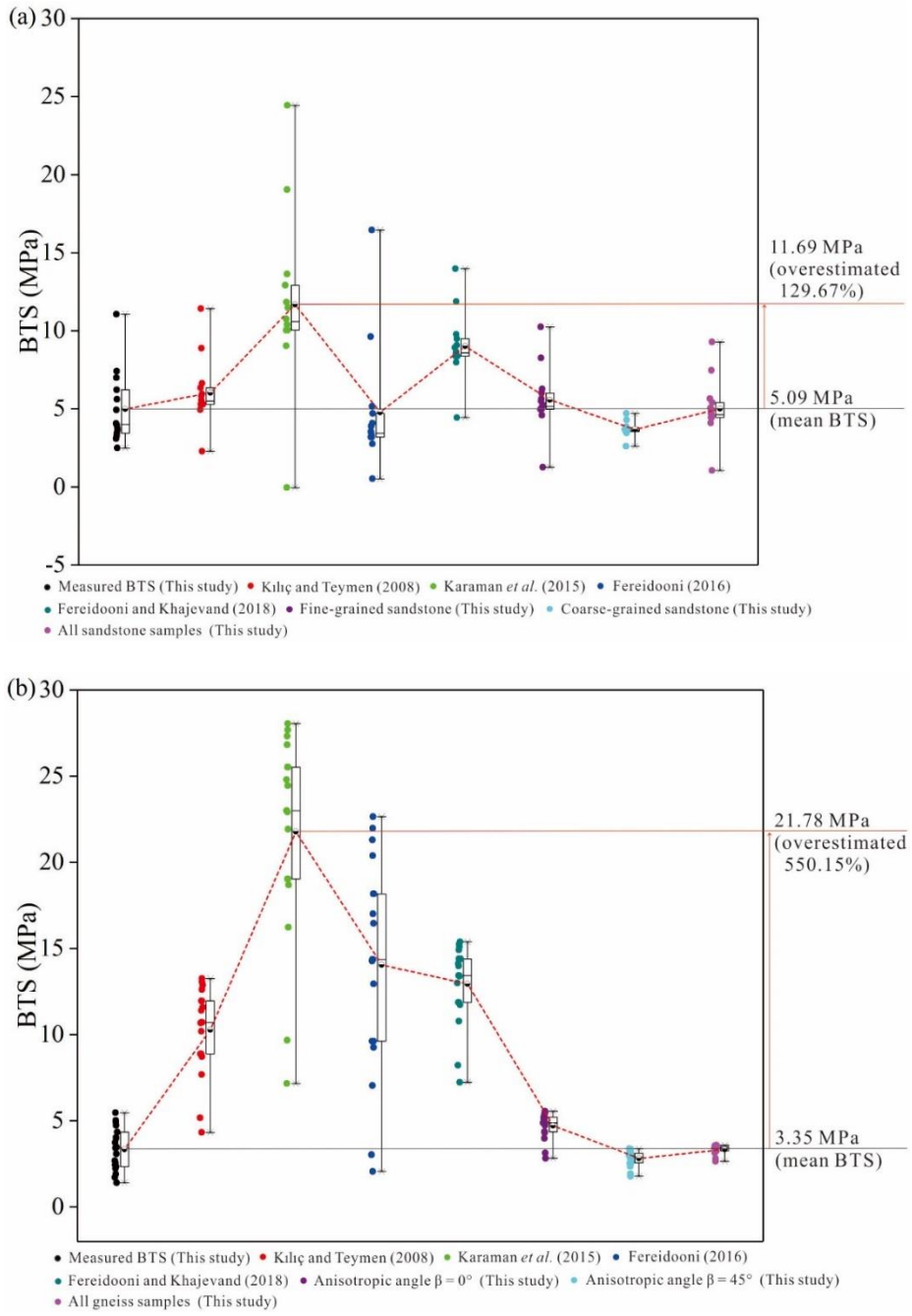

Fig. 12 Comparison between the proposed equations of BTS-*R* and previous studies. (a) sandstone samples; (b) gneiss samples

References

Aliyu, M.M., Shang, J., Murphy, W., Lawrence, J.A., Collier, R., Kong, F. and Zhao, Y.Z. (2019), "Assessing the uniaxial compressive strength of extremely hard cryptocrystalline flint", *Int. J. Rock Mech. Min. Sci*, **113**, 310-321. https://doi.org/10.1016/j.ijrmms.2018.12.002.

ASTM (2008), Standard test method for splitting tensile strength of intact rock core specimens (D3967-08), ASTM International; West Conshohocken, U.S.A.

Aydin, A. (2009), "ISRM suggested method for determination of the Schmidt hammer rebound hardness: revised version", *Int. J. Rock Mech. Min. Sci*, **46**(3), 627-634. https://doi.org/10.1016/j.ijrmms.2008.01.020.

Broch, E. (1983), "Estimation of strength anisotropy using the point-load test", *Int. J. Rock. Mech. Min. Sci*., **20**, 181-187. https://doi.org/10.1016/0148-9062(83)90942-7.

Butenuth, C. (1997), "Comparison of tensile strength values of rocks determined by point load and direct tension tests", *Rock. Mech. Rock. Eng.*, **30**, 65-72. https://doi.org/10.1007/BF01020114.

Cai, M., and Kaiser, P.K. (2005), "Assessment of excavation damaged zone using a micromechanics model", *Tunn. Undergr. Sp. Tech*., **20**, 301-310. https://doi.org/10.1016/j.tust.2004.12.002.

China Geological Survey (2019), Geological Cloud of China Geological Survey; China Geological, Survey Beijing, China. www.cgs.gov.cn.

China National Standard (2013), Standard for Test Methods of Engineering Rock Mass (GB/T 50266-2013), Ministry of Housing and Urban-Rural Development of the People's Republic of China; Beijing, China.

Erarslan, N. and Williams, D. J. (2012), "Experimental, numerical and analytical studies on tensile strength of rocks", *In. J. Rock. Mech. Min. Sci*, **49**, 21-30. https://doi.org/10.1016/j.ijrmms.2011.11.007.

Fereidooni, D. (2016), "Determination of the geotechnical characteristics of hornfelsic rocks with a particular emphasis on the correlation between physical and mechanical properties", *Rock. Mech. Rock. Eng.*, **49**(7), 2595-2608. https://doi.org/10.1007/s00603-016-0930-3.

Fereidooni, D. and Khajevand, R. (2018), "Determining the geotechnical characteristics of some sedimentary rocks from Iran with an emphasis on the correlations between physical, index, and mechanical properties", *Geotech. Test. J.*, **41**(3), 555-573. https://doi.org/10.1520/GTJ20170058.

Gurocak, Z., Solanki, P., Alemdag, S. and Zaman, M.M. (2012), "New considerations for empirical estimation of tensile strength of rocks", *Eng. Geol.*, **145-146**, 1-8. https://doi.org/10.1016/j.enggeo.2012.06.005.

Heidari, M., Khanlari, G.R., Kaveh, M.T. and Kargarian, S. (2012), "Predicting the uniaxial compressive and tensile strengths of gypsum rock by point load testing", *Rock. Mech. Rock. Eng.*, **45**(2), 265-273. https://doi.org/10.1007/s00603-012-0264-8.

ISRM (1978), "Suggested methods for determining tensile strength of rock materials", *Int. J. Rock. Mech. Min. Sci. Geomech. Abstr.*, **15**, 99-103. https://doi.org/10.1016/0148-9062(78)90003-7.

ISRM (2015), "ISRM Suggested method for determination of the Schmidt hammer rebound hardness: Revised version", *The ISRM Suggested methods for rock characterization, testing and monitoring: 2007-2014*, International Society for Rock Mechanics Commission on Testing Methods, London, U.K.

Jamshidi, A., Zamanian, H. and Sahamieh, R.Z. (2018), "The effect of density and porosity on the correlation between uniaxial compressive strength and P-wave velocity", *Rock. Mech. Rock. Eng.*, **51**(4), 1279-1286. https://doi.org/10.1007/s00603-017-1379-8.

Kahraman, S., Fener, M., Kasling, H. and Thuro, K. (2018), "Investigating the effect of strength on the LCPC abrasivity of igneous rocks", *Geomech. Eng.*, **15**(2), 805-810. https://doi.org/10.12989/gae.2018.15.2.805.

Karakul, H. and Ulusay, R. (2013), "Empirical correlations for predicting strength properties of rocks from P-wave velocity under different degrees of saturation", *Rock. Mech. Rock. Eng.*, **46**(5), 981-999. https://doi.org/10.1007/s00603-012-0353-8.

Karaman, K., Kesimal, A. and Ersoy, H. (2015), "A comparative assessment of indirect methods for estimating the uniaxial compressive and tensile strength of rocks", *Arab. J. Geosci.*, **8**(4), 2393-2403. https://doi.org/10.1007/s12517-014-1384-0.

Khandelwal, M. (2013), "Correlating P-wave velocity with the physico-mechanical properties of different rocks", *Pure. Appl. Geophys.*, **170**(4), 507-514. https://doi.org/10.1007/s00024-012-0556-7.

Khandelwal, M. and Singh, T.N. (2009), "Correlating static properties of coal measures rocks with p-wave velocity", *Int. J. Coal. Geol.*, **79**, 55-60. https://doi.org/10.1016/j.coal.2009.01.004.

Khanlari, G.R., Heidari, M., Sepahi-Gero, A.A. and Fereidooni, D. (2014), "Quantification of strength anisotropy of metamorphic rocks of the Hamedan province, Iran, as determined from cylindrical punch, point load and Brazilian tests", *Eng. Geol.*, **169**, 80-90. https://doi.org/10.1016/j.enggeo.2013.11.014.

Khanlari, G.R., Heidari, M., Sepahi-Gero, A.A. and Fereidooni, D. (2014), "Determination of geotechnical properties of anisotropic rocks using some index tests", *Geotech. Test. J.*, **37**(2), 242-254. https://doi.org/10.1520/GTJ20130078.

Kılıç, A. and Teymen, A. (2008), "Determination of mechanical properties of rocks using simple methods", *Bull. Eng. Geol. Environ*, **67**, 237-244. https://doi.org/10.1007/s10064-008-0128-3.

Komurlu, E., Kesimal, A. and Demir, A.D. (2017), "Dog bone shaped specimen testing method to evaluate tensile strength of rock materials", *Geomech. Eng.*, **12**(6), 883-898. https://doi.org/10.12989/gae.2017.12.6.883.

Komurlu, E., Kesimal, A. and Demir, S. (2016), "Experimental and numerical analyses on determination of indirect (splitting) tensile strength of cemented paste backfill materials under different loading apparatus", *Geomech. Eng.*, **10**(6), 775-791. http://doi.org/10.12989/gae.2016.10.6.775.

Kong, F. and Shang, J. (2018), "A validation study for the estimation of Uniaxial Compressive Strength based on index tests", *Rock. Mech. Rock. Eng*, **51**(7), 2289-2297. https://doi.org/10.1007/s00603-018-1462-9.

Kong, F., Xue, Y., Qiu, D., Gong, H., and Ning, Z. (2021), "Effect of grain size or anisotropy on the correlation between uniaxial compressive strength and Schmidt hammer test for building stones", *Constr. Build. Mater.*, **299**, 123941. https://doi.org/10.1016/j.conbuildmat.2021.123941.

Kumari, W., Beaumont, D.M., Ranjith, P.G., Perera, M., Avanthi Isaka, B.L. and Khandelwal, M. (2019), "An experimental study on tensile characteristics of granite rocks exposed to different high-temperature treatments", *Geomech. Geophys. Geol.*, **5**, 47-64. https://doi.org/10.1007/s40948-018-0098-2.

Li, D. and Wong, L.N.Y. (2013), "Point load test on meta-sedimentary rocks and correlation to UCS and BTS", *Rock. Mech. Rock. Eng.*, **46**(4), 889-896. https://doi.org/10.1007/s00603-012-0299-x.

Liu, C., Deng, H., Zhao, H. and Zhang, J. (2018), "Effects of freeze-thaw treatment on the dynamic tensile strength of granite using the Brazilian test", *Cold. Reg. Sci. Technol.*, **155**, 327-332. https://doi.org/10.1016/j.coldregions.2018.08.022.

Liu, J., Chen, L., Wang, C., Man, K., Wang, L., Wang, J. and Su, R. (2014), "Characterizing the mechanical tensile behavior of Beishan granite with different experimental methods", *Int. J. Rock. Mech. Min. Sci.*, **69**, 50-58. https://doi.org/10.1016/j.ijrmms.2014.03.007.

Mishra, D.A. and Basu, A. (2012), "Use of the block punch test to predict the compressive and tensile strengths of rocks", *Int. J. Rock. Mech. Min. Sci.*, **51**, 119-127. https://doi.org/10.1016/j.ijrmms.2012.01.016.

OriginLab, (2019), Regression and curve Fitting-Interpreting Regression Results; OriginLab Corporation, Northampton, USA. www.originlab.com/doc/Origin-Help/Interpret-Regression-Result#Prob.3EF.

Perras, M.A. and Diederichs, M.S. (2014), "A review of the tensile strength of rock: concepts and testing", *Geotech. Geol. Eng.*, **32**(2), 525-546. https://doi.org/10.1007/s10706-014-9732-0.

Roy, D. G., and Singh, T.N. (2016), "Effect of heat treatment and layer orientation on the tensile strength of a crystalline rock under brazilian test condition", *Rock. Mech. Rock. Eng.*, **49**(5), 1663-1677. https://doi.org/10.1007/s00603-015-0891-y.

Roy, D.G., Singh, T.N., Kodikara, J. and Das, R. (2017), "Effect of water saturation on the fracture and mechanical properties of sedimentary rocks", *Rock. Mech. Rock. Eng.*, **50**(10), 2585-2600. https://doi.org/ 10.1007/s00603-017-1253-8.

Shang, J. (2020), "Rupture of veined granite in polyaxial compression: insights from three-dimensional discrete element method modeling", *J. Geophys. Res-Sol. Ea.*, **125**(2), 2019JB019052. https://doi.org/10.1029/2019JB019052.

Shang, J., Hencher, S.R. and West, L.J. (2016), "Tensile strength

of geological discontinuities including incipient bedding, rock joints and mineral veins", *Rock. Mech. Rock. Eng.*, **49**(11), 4213-4225. https://doi.org/10.1007/s00603-016-1041-x.

Shen, B. and Barton, N. (2018), "Rock fracturing mechanisms around underground openings", *Geomech. Eng.*, **16**(1), 35-47. https://doi.org/10.12989/gae.2018.16.1.035.

Singh, P.K., Tripathy, A., Kainthola, A., Mahanta, B., Singh, V. and Singh, T.N. (2017), "Indirect estimation of compressive and shear strength from simple index tests", *Eng. Comput.*, **33**(1), 1-11. https://doi.org/10.1007/s00366-016-0451-4.

Sirdesai, N.N., Singh, T.N., Ranjith, P.G. and Singh, R. (2016), "Effect of varied durations of thermal treatment on the tensile strength of red sandstone", *Rock. Mech. Rock. Eng.*, **50**(1), 1-9. https://doi.org/10.1007/s00603-016-1047-4.

Tutmez, B. (2017), "Comparison of measurement uncertainty calculation methods on example of indirect tensile strength measurement", *Geomech. Eng.*, **12**(6), 871-882. https://doi.org/10.12989/gae.2017.12.6.919.

Wang, Y. and Hu, X. (2017), "Determination of tensile strength and fracture toughness of granite using notched three-point-bend samples", *Rock. Mech. Rock. Eng.*, **50**(1), 17-28. https://doi.org/10.1007/s00603-016-1098-6.

Wang, Z.L., Li, Y.C. and Shen, R.F. (2007), "Numerical simulation of tensile damage and blast crater in brittle rock due to underground explosion", *Int. J. Rock. Mech. Min. Sci*, **44** 730-738. https://doi.org/10.1016/j.ijrmms.2006.11.004.

Wei, K., Ouyang, C., Duan, H., Li, Y., Chen, M., Ma, J., An, H. and Zhou, S. (2020), "Reflections on the catastrophic 2020 Yangtze River Basin flooding in southern China", *Innovation*, **1**(2), 10038. https://doi.org/10.1016/j.xinn.2020.100038.

Xia, K., Yao, W. and Wu, B. (2017), "Dynamic rock tensile strengths of Laurentian granite: Experimental observation and micromechanical model", *J. Rock. Mech. Geotech. Eng.* **9**(1) 116-124. https://doi.org/10.1016/j.jrmge.2016.08.007.

Xue, Y., Kong, F., Li, S., Zhang, L., Zhou, B., Li, G. and Gong, H. (2020), "Using indirect testing methods to quickly acquire the rock strength and rock mass classification in tunnel engineering", *Int. J. Geomech.*, **20**(5), 05020001. https://doi.org/10.1061/(ASCE)GM.1943-5622.0001633.

Xue, Y., Kong, F., Li, S., Zhang, Q., Qiu, D., Su, M. and Li, Z. (2021), "China starts the world's hardest "Sky-High Road" project: Challenges and countermeasures for Sichuan-Tibet railway", *The Innovation*, **2**(2), 100105. https://doi.org/10.1016/j.xinn.2021.100105.

Yao, W., Xia, K. and Li, X. (2018), "Non-local failure theory and two-parameter tensile strength model for semi-circular bending tests of granitic rocks", *Int. J. Rock. Mech. Min. Sci.*, **110**, 9-18. https://doi.org/10.1016/j.ijrmms.2018.07.002.

Yilmaz, I. (2010), "Use of the core strangle test for tensile strength estimation and rock mass classification", *Int. J. Rock. Mech. Min. Sci*., **47**(5), 845-850. https://doi.org/10.1016/j.ijrmms.2010.03.003.

Zhao, Z., Yang, J., Zhang, D. and Peng, H. (2017), "Effects of wetting and cyclic wetting-drying on tensile strength of sandstone with a low clay mineral content", *Rock. Mech. Rock. Eng.*, **50**(2), 485-491. https://doi.org/10.1007/s00603-016-1087-9.